RSC Advances

ROYAL SOCIETY OF CHEMISTRY

www.rsc.org/advances

Effect of A/B-site Substitution on Oxygen Production Performance of Strontium Cobalt Based Perovskites for CO_2 Capture Application

Qiuwan Shen [a,b], Ying Zheng [a,*], Cong Luo [a], Ning Ding [c], Chu-Guang Zheng [a], Marcus Thern[b,*]

[a] State Key Laboratory of Coal combustion, Huazhong University of Science &Technology, Wuhan 430074, China
[b] Department of Energy Sciences, Lund University, P.O. Box 118 , SE-221 00 Lund , Sweden
[c] Energy Research Institute of Shandong Academy of Sciences , Jinan 250014, China

Abstract: Oxy-fuel combustion is one of the proposed technologies which have the potential to achieve a zero CO_2 emission. Strontium cobalt based perovskite oxygen carriers are promising materials for air separation with a high selectively for oxygen. And these perovskites can producing an oxygen enriched carbon dioxide stream for oxyfuel combustion process. The relative low oxygen production yield may be a drawback of this type of materials for this technology. This paper presents an effective approach by A/B-site substitution to improve the oxygen production performance of the perovskites. In this study, a series of different A/B-site substituted $SrCo_{0.8}Fe_{0.2}O_{3-\delta}$ were prepared by an EDTA-citrate sol-gel combustion synthesis method. Fixed-bed experiments and TGA measurements were performed to study the effects of A/B-site substitution on cyclic oxygen adsorption/desorption performance of the synthesized samples. The experimental results indicate that the oxygen desorption amount of different A-site substituted perovskites decrease in the order of $BaCo_{0.8}Fe_{0.2}O_{3-\delta}$ > $Ba_{0.5}Sr_{0.5}Co_{0.8}Fe_{0.2}O_{3-\delta}$ > $SrCo_{0.8}Fe_{0.2}O_{3-\delta}$ > $Sr_{0.5}Ca_{0.5}Co_{0.8}Fe_{0.2}O_{3-\delta}$ > $MgCo_{0.8}Fe_{0.2}O_{3-\delta}$. Moreover, B-site substitution by different transition metal ions can significantly modified oxygen adsorption capacity and oxygen desorption performance of $SrCo_{0.8}Fe_{0.2}O_{3-\delta}$. Furthermore, oxygen desorption performance can be improved when

Corresponding author. Tel.: +86 27-63120550. +46 462224112
E-mail address: Y.Zheng1967@gmail.com (Y. Zheng). Marcus.Thern@energy.lth.se(M.Thern)

Fe ions of the perovskite $SrCo_{0.8}Fe_{0.2}O_{3-\delta}$ were substituted by Zr, Cr, Zn, Ni ions.

Key words: Perovskite-type; $SrCo_{0.8}Fe_{0.2}O_{3-\delta}$; A/B-site substitution; Oxygen adsorption/desorption

1. Introduction

It is acknowledged that the combustion of fossil fuels contributes to the emission of CO_2 into the atmosphere, which in turn causes global warming [1-3]. Oxy-fuel combustion is one of the proposed technologies which have the potential to achieve a zero CO_2 emission. Oxy-fuel combustion is well known as the O_2/CO_2 recycle combustion process, in which oxygen is fed to the combustion chamber, and a major part of the CO_2 rich exhaust gas is recycled back to maintain the combustion temperature. Although the oxy-fuel combustion process offers obvious advantages over regular combustion processes, one of the key barriers to implementation of oxy-combustion, however, is the cost of producing the oxygen. Therefore, significant reduction in the cost of oxygen production is a key requirement in making the oxy-fuel combustion power plant a viable future option when carbon dioxide capture becomes a necessity [4-5].

Perovskite-type metal oxides have been receiving increasing attention for a wide variety of applications, such as a component of capacitors, microwave technology, varistors, electrodes, and immobilization of nuclear wastes, as well as being catalysts for oxidation and hydrogenation [6-9]. Perovskite-type metal oxides have the general formula ABO_3, where A-site can be an alkali, alkine earth, rare earth or other large ion,

and B-site can be transitional metal ion. If A- and/or B-sites are substituted with lower valent cations, in order to maintain charge neutrality, some oxygen ions are removed from the lattice thereby creating oxygen vacancies [10]. Perovskite metal oxides have excellent mixed ionic-electronic conductivity and exhibit extremely high selectivity for oxygen due to the existence of oxygen vacancies. Perovskites are highly selective for oxygen over nitrogen or other non-oxygen containing gases which makes them ideal candidates as oxygen permeable membrane. However, this technology faces major challenges in regard to the scale-up manufacturing and stability of the membranes [11].

Lin et al. proposed a new process of producing pure O_2 or O_2/CO_2 gas streams by using a perovskite-type oxygen carrier in oxy-fuel combustion [11]. A general scheme of such a process is shown in Figure 1: (1) oxygen adsorption in air reactor; (2) oxygen desorption in CO_2 reactor. For oxygen adsorption step, air is used as feed gas to saturate the perovskite oxygen carrier with O_2; while in the oxygen desorption step, using CO_2 as a sweep gas to desorb O_2 from the perovskite to produce an O_2-enriched CO_2 flue gas stream. The reversible adsorption/desorption processes based on the perovskite-type oxygen carrier is described as below [12]:

$$2ABO_{3-\delta} + 2CO_2 \Leftrightarrow 2ACO_3 + B_2O_3 + \frac{1-2\delta}{2}O_2 \quad (1)$$

Relative low oxygen desorption amount may be a major drawback of this type of materials for this technology. This issue may cause challenges to achieving a high efficiency of O_2 product amount in practical application. Therefore, improving the

oxygen desorption performance is of great importance to develop the promising perovskite for oxygen production.

A common approach to improve the properties of perovskite-type oxygen carrier is through A/B site substitution in the metal oxides. $SrCo_{1-x}Fe_xO_{3-\delta}$ is a promising perovskite that has drawn considerable attention because of its high oxygen permeability [13-14].

This paper is an extension of our previous study [14]. We found that the oxygen production performance of $SrCo_{1-x}Fe_xO_{3-\delta}$ is improved by Co doping. $SrCo_{0.8}Fe_{0.2}O_{3-\delta}$ has the best oxygen production property among the $SrCo_{1-x}Fe_xO_{3-\delta}$ (x= 0.2, 0.4, 0.6, 0.8) and multiple cycles demonstrated that $SrCo_{0.8}Fe_{0.2}O_{3-\delta}$ also displays high stability and regeneration capacity. The present work was focused on understanding the effects of A/B site substitution in $SrCo_{0.8}Fe_{0.2}O_{3-\delta}$ perovskite on its oxygen production performance.

2. Experimental

2.1. Materials and Preparation Method

Perovskite samples used in this study were synthesized by an EDTA-citrate sol-gel combustion synthesis [15-20]. The starting materials were $Sr(NO_3)_2 \cdot 4H_2O$, $Co(NO_3)_2 \cdot 6H_2O$, Fe $(NO_3)_3 \cdot 9H_2O$, citric acid and ethylenediamine-tetraacetic acid (EDTA), all of which were of analytical purity. As for synthesizing 0.1 mol of $SrCo_{0.8}Fe_{0.2}O_{3-\delta}$ powders, the detail procedures are described as follows: First, 0.1 mol of EDTA was mixed with 125 ml of 13 N NH_4OH solutions to make a NH_3-EDTA solution. Then, 0.05 mol of $Sr(NO_3)_2 \cdot 4H_2O$,0.04 mol of $Co(NO_3)_2 \cdot 6H_2O$ and 0.01

mol of $Fe(NO_3)_3 \cdot 9H_2O$ were dissolved to the NH_3-EDTA solution. The solution was mixed and stirred, then 0.15 mol of citric acid was added to the mixed solution. The mole ratios of EDTA: citric acid: total metal ions were 1:1.5:1. Then the precursor solution was heated and stirred at 70 ℃ until it gelled. The resulting viscous gel was dried at 105℃ for 24 h and self-ignited at 400 ℃ or 4 h to burn out the organic compounds. Finally, the black ash was sintered at 850 ℃ for 20 h and ground into fine powders for characterization.

2.2. Fixed-bed experiments and TGA measurements

Oxygen adsorption/desorption experiments were performed in a fixed-bed reactor system as shown in Figure 2. It consisted of a gas feeding system, a tube furnace with a quartz reactor, a gas analyzer (Gasboard 3100) and a computerized data-acquisition system. Oxygen concentration during desorption process were recorded to investigate the oxygen production performance of perovskite powders. About 1.0 g of powders was packed in the middle of the quartz reactor. Air and CO_2 were respectively used as the feed gas for adsorption step and sweep gas for desorption step.

In the adsorption step, the powders were heated to a desired adsorption temperature in a flow of air in 1 atm at flow rate of 200 ml/min for 10 min. The adsorption step was followed by the desorption step with a switch of the sweep gas from Air to CO_2 stream at a flow rate of 50 ml/min, and setting the temperature to the predetermined desorption temperature. The desorption step was stopped when the O_2 concentration nearly dropped to zero. Then the CO_2 stream was switched to air to start

the next cycle of oxygen adsorption and desorption processes.

The detailed oxygen adsorption properties of perovskite were also studied by thermogravmeteric analysis (DSC/TGA, STA449C) in a temperature range 25-850 ℃ ℃ at a constant gas flow rate of 80 ml/min and the heating rate was 15 ℃/min. For a typical TGA measurement, approximately 10 mg of dry powder was placed in an alumina crucible. The sample was heated to the designed temperature in 1 atm atmosphere (air or N_2) and until a stable weight was observed from the TGA curve. The feed gas was switched quickly between the air and N_2. Weight change was recorded continuously by TGA analysis.

3. Results and discussions

3.1 Effects of A-site substitution on oxygen adsorption/desorption performance

Figure 3 compares the oxygen adsorption breakthrough curves of different A-site total/partial substituted $SrCo_{0.8}Fe_{0.2}O_{3-\delta}$ perovskite samples denoted as $SrCo_{0.8}Fe_{0.2}O_{3-\delta}$ (SCF), $BaCo_{0.8}Fe_{0.2}O_{3-\delta}$(BCF), $Ba_{0.5}Sr_{0.5}Co_{0.8}Fe_{0.2}O_{3-\delta}$ (BSCF), $Sr_{0.5}Ca_{0.5}Co_{0.8}Fe_{0.2}O_{3-\delta}$ (SCCF) and $MgCo_{0.8}Fe_{0.2}O_{3-\delta}$ (MCF) at the air flow rate of 200 ml/min at 850 ℃. A standard oxygen adsorption breakthrough curve was introduced for comparison. The results show that the breakthrough curves are similar in shape with a sharp increase after a breakthrough time (50-100 s), and soon afterward all the curves are characterized by a long tail. For example, for BSCF, no outgoing oxygen was detected by the oxygen sensor before 100 s, and after 150 s, the outlet oxygen concentration was equal to the feed gas concentration (20.9 %). Figure 3 indicates that MCF sample have the shortest breakthrough time (oxygen adsorption capacity), on the contrary,

BSCF have the longest breakthrough time.

Figure 4 depicts the comparison of oxygen desorption curves of SCF with different A-site total/partial substitution. It is clear that A-site total/partial substitution has significant influence on oxygen desorption properties of SCF. Oxygen desorption amount of each desorption process shown in Figure 4 for different samples are given in Table 1. The oxygen desorption amount was calculated by the integral scheme based on the obtained oxygen concentration distribution. The following equation can be used:

$$m_{O_2} = \frac{\Sigma C_{O_2} \times F_{out} \times M_{O_2}}{V_m \times m} \quad (2)$$

where ΣC_{O_2} is the integration of the entire oxygen concentration during desorption and F_{out} (ml/s) is the flow rate of desorption effluent. We suppose that $F_{out} \approx F_{CO_2}$, M_{O_2} (g/mol) is the molecular weight of O_2, m (g) is the mass of perovskite sample, and m_{O_2} (g/g·sample) is the oxygen desorption amount for 1 g of perovskite sample.

The results show that oxygen desorption amount is in the order BCF>BSCF>SCF>SCCF>MCF. It is also can be seen from Figure 4 that the slope of the curves of BCF and BSCF are bigger than others which demonstrate the oxygen desorption rates of BCF and BSCF are faster than the rest. The outlet oxygen concentration of BCF reached the maximum value of 25 % after 150 s. On the other hand, substitution of Sr^{2+} with Ca^{2+}/Mg^{2+} reduces the oxygen desorption amount for $SrCo_{0.8}Fe_{0.2}O_{3-\delta}$. The lower desorption amount may be related to the smaller ionic radius, as ionic radius is in the order Ba(1.75Å)>Sr(1.58Å)>Ca(1.48Å)>Mg (1.03Å),

the bigger ionic radius of Ba resulting in the increase of lattice volume and leading contribution to oxygen ions transition in the crystal. Therefore, though high temperature oxygen (β-oxygen) desorption is usually related to the B-site substitution, it is also affected by A-site substitution [21]. Moreover， for a fixed B-site composition,A-site ionic with the same valency but different ionic radius affects the oxygen desorption property.

Table 1 oxygen desorption amount of a unit mass of A(A=Sr, Ba, Mg, Ca)$Co_{0.8}Fe_{0.2}O_{3-\delta}$

Samples	BCF	BSCF	SCF	SCCF	MCF
Time range to collect the product in desorption（t1~t2）	128s-400s	126s-400s	143s-400s	143s-400s	135s-400s
Oxygen desorption amount (mg O_2 /g·sample)	45.5	35.8	33.0	31.5	10.2

3.2 Effects of fixed-bed operation condition on oxygen production performance

3.2.1 Desorption temperature

Figure 5 presents the desorption curves of $BaCo_{0.8}Fe_{0.2}O_{3-\delta}$ at different desorption temperatures from 750 ℃ to 950 ℃ (with the same adsorption temperature at 850 ℃). As shown in Figure 5, it is clear that 850 ℃ is the ideal desorption temperature for $BaCo_{0.8}Fe_{0.2}O_{3-\delta}$. It is known that the carbonation reaction between CO_2 and $BaCo_{0.8}Fe_{0.2}O_{3-\delta}$ is a typical gas-solid reaction. The higher desorption temperature contributes to the higher carbonation rates which can produce more oxygen in the desorption process. However, when the temperature is higher than 900 ℃ ， the oxygen desorption performance of $BaCo_{0.8}Fe_{0.2}O_{3-\delta}$ begins to fall. It

might be caused by the decrease of the sample surface area during the carbonation reaction. Therefore an optimum oxygen desorption temperature exist in the oxygen desorption process.

3.2.2 CO_2 partial pressure

In the carbonation reaction of perovskite with CO_2, except for desorption temperature, partial pressure in gas phase also plays a key role in the desorption process. Figure 6 shows desorption curves at different CO_2 partial pressure during the desorption process of $BaCo_{0.8}Fe_{0.2}O_{3-\delta}$ at 850 °C. As shown in Figure 6, a higher CO_2 partial pressure leads to a larger amount of oxygen produces in the desorption process. The carbonation reaction of $BaCo_{0.8}Fe_{0.2}O_{3-\delta}$ perovskite-type oxygen carriers with CO_2 is described as follows:

$$BaCo_{0.8}Fe_{0.2}O_{3-\delta} + CO_2 \Leftrightarrow BaCO_3 + 0.8CoO + 0.1Fe_2O_3 + \frac{0.9-\delta}{2}O_2 \quad (3)$$

It is clear that the pressure dependence of carbonation reaction for $BaCo_{0.8}Fe_{0.2}O_{3-\delta}$ is consistent with the known properties of gas-solid reaction [13]. The mass-action law demonstrates that the carbonation reaction rate (oxygen desorption rate) increase with CO_2 partial pressure.

3.3 Effects of B-site substitution on oxygen adsorption/desorption performance

Effects of B-site substitution by different transition metal ions on oxygen adsorption/desorption performance of $SrCo_{0.8}B_{0.2}O_3$ (B=Ni,Zn,Zr,Cr,Cu,Fe) were studied. Oxygen adsorption capacities of all the samples were investigated by TGA

analysis. Based on the weight change measurement by TGA, the oxygen adsorption capacities under a given temperature can be calculate by:

$$q = \frac{1}{2M_O}\frac{W_{air} - W_{N_2}}{W_0} \quad (4)$$

where q is the oxygen adsorption capacity (mol/g); *Mo* is the molecular weight of O; W_{air} (g) and W_{N2}(g) is the equilibrium weight in air and N_2 at particular temperature, respectively; W_0 is the weight of the sample at initial condition (110 ℃ in 1 atm air).

Equilibrium weight (mg) of $SrCo_{0.8}B_{0.2}O_{3-\delta}$ (B=Fe, Ni, Cu, Zn, Cr, Zr) at different conditions were listed in Table 2. Figure 7 compares the oxygen adsorption capacity which was calculated from data in Table 2. The results show that the substitution of Fe by Zr, Cr and Cu in $SrCo_{0.8}B_{0.2}O_{3-\delta}$ increases the oxygen adsorption capacity, the adsorption capacity decreases in the order $SrCo_{0.8}Zr_{0.2}O_{3-\delta}$ (Sr-Co-Zr)> $SrCo_{0.8}Cr_{0.2}O_{3-\delta}$ (Sr-Co-Cr)>$SrCo_{0.8}Cu_{0.2}O_{3-\delta}$(Sr-Co-Cu)>$SrCo_{0.8}Fe_{0.2}O_{3-\delta}$ (Sr-Co-Fe)> $SrCo_{0.8}Ni_{0.2}O_{3-\delta}$(Sr-Co-Ni)>$SrCo_{0.8}Zn_{0.2}O_{3-\delta}$(Sr-Co-Zn).

Generally speaking, substitution of B-site by higher valent cations, such as Zr,Cr results in less adsorption capacity because the charge neutrality rule restrains the formation of oxygen vacancy. Since the results contradicts the results of this study, it may appear that except for oxygen vacancy of perovskite, the oxygen adsorption capacity also relates to the surface adsorption activity.

Table 2 Equilibrium weight (mg) of $SrCo_{0.8}B_{0.2}O_{3-\delta}$ (B=Fe,Ni,Cu,Zn,Cr,Zr) at initial conditions, and 850 °C in air and N_2, respectively.

Samples	Sr-Co-Ni	Sr-Co-Zn	Sr-Co-Zr	Sr-Co-Cr	Sr-Co-Cu	Sr-Co-Fe

$W_{air(mg)}$	10.500	10.400	8.969	9.319	9.372	9.655
$W_{N2(mg)}$	10.465	10.370	8.907	9.259	9.314	9.615
$W_{0(mg)}$	10.67	10.64	9.789	9.646	9.563	9.867

Figure 8 shows a comparison of cyclic oxygen desorption performance for $SrCo_{0.8}B_{0.2}O_{3-\delta}$ (B=Fe, Ni, Cu, Zn, Cr, Zr). It indicates that substitution of Fe in B-site with different transition metal ions has significantly effects on the oxygen desorption performance. The substitution of Fe by by Zr, Ni, Zn and Cr in $SrCo_{0.8}Fe_{0.2}O_{3-\delta}$ enhanced the oxygen desorption amount. On the other hand, substitution of Fe by Cu reduced the oxygen desorption amount which results in the lowest cyclic ability for $SrCo_{0.8}Cu_{0.2}O_{3-\delta}$ among the samples as showed in Figure 8. These results indicate that substitution of Fe with Zr and Cr in $SrCo_{0.8}Fe_{0.2}O_{3-\delta}$ enhanced both oxygen adsorption capacity and desorption amount; substitution with Zn and Ni increased the oxygen desorption amount but adversely reduced the oxygen adsorption capacity. Considering both the adsorption/desorption, the performance of $SrCo_{0.8}Zr_{0.2}O_{3-\delta}$ was the best followed by $SrCo_{0.8}Cr_{0.2}O_{3-\delta}$ among the different composition of $SrCo_{0.8}B_{0.2}O_{3-\delta}$ with different B-site transition metal iron substitution.

4. Conclusions

In this study, oxygen production performance of a new series strontium cobalt based perovskites with A/B-site substitution was investigated. The following conclusions can be drawn from this study:

1. Oxygen desorption amount of different A-site substituted perovskites decrease in

the order of $BaCo_{0.8}Fe_{0.2}O_{3-\delta}$ > $Ba_{0.5}Sr_{0.5}Co_{0.8}Fe_{0.2}O_{3-\delta}$ > $SrCo_{0.8}Fe_{0.2}O_{3-\delta}$ > $Sr_{0.5}Ca_{0.5}Co_{0.8}Fe_{0.2}O_{3-\delta}$ > $MgCo_{0.8}Fe_{0.2}O_{3-\delta}$. The lower desorption amount is related to the smaller ionic radius, the bigger ionic radius of Ba resulting in the increase of lattice volume and leading contribution to oxygen ions transition in the crystal.

2. B-site substitution by different transition metal ions can significantly modified oxygen adsorption capacity and oxygen desorption performance of $SrCo_{0.8}Fe_{0.2}O_{3-\delta.}$ Fe substituted by Zr,Cr and Cu in $SrCo_{0.8}B_{0.2}O_{3-\delta}$ increasing the oxygen adsorption capacity, it may appear that except for oxygen vacancy of perovskite, the oxygen adsorption capacity is also related to the surface adsorption activity. Moreover, substitution of Fe ion in $SrCo_{0.8}Fe_{0.2}O_{3-\delta}$ with Zr,Ni,Zn and Cr ions all enhanced the oxygen desorption amount. On the contrary, substitution a Fe ion with Cu reduced the oxygen desorption amount. Considering both the adsorption/desorption, the performance of $SrCo_{0.8}Zr_{0.2}O_{3-\delta}$ was the best followed by $SrCo_{0.8}Cr_{0.2}O_{3-\delta}$ among the different composition of $SrCo_{0.8}B_{0.2}O_{3-\delta}$ with different B-site transition metal iron substitution.

Acknowledgment

The authors acknowledge the financial supports of National Natural Science Foundation of China (No.51276078), and the National Basic Research Program of China (No.2011CB707301). The authors also gratefully acknowledge the financial supports from China Scholarship Council

259

260 **References**

261 1. Q.W. Shen, Y. Zheng, C. Luo, and C.G. Zheng. Development and
262 characterization of $Ba_{1-x}Sr_xCo_{0.8}Fe_{0.2}O_{3-\delta}$ perovskite for oxygen production in
263 oxyfuel combustion system, *Chem. Eng. J.* 2014, **225**, 462-470.
264 2. B. W. Wang, G. Xiao, X. Y. Song, H.B. Zhao, C.G.Zheng, Chemical looping
265 combustion of high-sulfur coal with $NiFe_2O_4$-combined oxygen carrier, *J Therm.*
266 *Anal. Calorim.* 2014,**118**, 1593-1602.
267 3. C. Luo, Y. Zheng, J. J. Yin, C. L. Qin, N. Ding, C. G. Zheng, B. Feng, Effect of
268 sulfation during oxy-fuel calcination stage in calcium looping on CO_2 capture
269 performance of CaO-based sorbent, *Energy Fuels* 2013,**27**,1008-1014.
270 4. E. Croiset, K. V. Thambimuthu, NO_x and SO_2 emissions from O_2/CO_2 recycle
271 coal combustion, *Fuel* 2001, **80**, 2117-2121.
272 5. B.J.P. Buhre, L. K. Elliott, C. D. Sheng, R. P. Gupta, T. F.Wall, Oxy-fuel
273 combustion technology for coal-fired power generation, *Prog. Energy Combust.*
274 *Sci.* 2005, **31**, 283-307.
275 6. M. Sun, X. W. Chen and L. Hong. Leveraging the A-site Ba^{2+}–Sr^{2+} ratio in the
276 designated perovskite to enhance oxygen transport and structural/interfacial
277 stability. *RSC Adv.,* 2014, **4**, 5618-5625.

7. H.J. Zhan, F. Li, P. Gao, N. Zhao, F.K. Xiao, W. Wei and Y.H. Sun, Influence of element doping on La–Mn–Cu–O based perovskite precursors for methanol synthesis from CO_2/H_2 .*RSC Adv.*, 2014, **4**, 48888-48896.

8. K. Zhang, J.K. Sunarso, Z.P. Shao, W. Zhou, C.H. Sun, S.B. Wang and S.M. Liu. Research progress and materials selection guidelines on mixed conducting perovskite-type ceramic membranes for oxygen production. *RSC Adv*, 2011, **1**, 1661–1676.

9. C. Zhang, R. Ran, G.H. Pham, K. Zhang, J. Liu and S. M. Liu. $Ce_{0.9}Gd_{0.1}O_{2-\delta}$ membranes coated with porous $Ba_{0.5}Sr_{0.5}Co_{0.8}Fe_{0.2}O_{3-\delta}$ for oxygen separation. *RSC Adv*, 2015, **5**, 5379-5386.

10. N. O. Vitoriano , C. B. López , I. R. Larramendi , R. Knibbe , K. Thydén , A. Hauch , P. Holtappels , T. Rojo , Optimizing solid oxide fuel cell cathode processing route for intermediate temperature operation, *Applied Energy* 2014,**104**, 984-991.

11. S. Guntuka, S. Banerjee, S. Farooq, M. P. Srinivasan, A- and B-site substituted lanthanum cobaltite perovskite as high temperature oxygen sorbent, *Ind. Eng. Chem. Res.* 2008, **47**, 154-162.

12. Z. Yang, Y. S. Lin, High-temperature sorption process for air separation and oxygen removal, *Ind. Eng. Chem. Res.* 2002, **41**, 2775-2784.

13. Q. Yang, Y. S. Lin, Improved sorbent for high-temperature production of oxygen-enriched carbon dioxide stream. *Ind. Eng. Chem. Res.* 2007, **46**, 6025-6031.

14. Z. B. Rui, J. J.Ding, Y. D. Li, $SrCo_{0.8}Fe_{0.2}O_{3-\delta}$ sorbent for high-temperature production of oxygen-enriched carbon dioxide atream, *Fuel* 2010,**89**, 1429-1434.

15. Q. W. Shen, Y. Zheng, C. Luo, and C.G. Zheng, Characteristics of $SrCo_{1-x}Fe_xO_{3-\delta}$ perovskite powders with improved O_2/CO_2 production performance for oxyfuel combustion, *Bull. Korean. Chem. Soc.* 2014, **35**, 1613-1616.

16. A. A. Yaremchenko, E. V. , A. V. Kovalevsky et al., Stability, oxygen permeability and chemical expansion of $Sr(Fe,Al)O_{3-\delta}$- and studies of $Sr(Co,Fe)O_{3-\delta}$- based membranes, *Solid State Ionics* 2011,**192**, 259-268.

17. H. Patra, S. K. Rout, S. K. Pratihar, S. Bhattacharya, Effect of process parameters on combined EDTA–citrate synthesis of $Ba_{0.5}Sr_{0.5}Co_{0.8}Fe_{0.2}O_{3-\delta}$ perovskite, *Powder Technol.* 2011,**209**, 98-104.

18. Z. Shao, S. M. Haile, A high-performance cathode for the next generation of solid-oxide fuel cells, *Nature* 2004, **431**,170-173.

19. H. Wang, C. Tablet, A. Feldhoff, J. Caro, Investigation of phase structure, sintering, and permeability of perovskite-type $Ba_{0.5}Sr_{0.5}Co_{0.8}Fe_{0.2}O_{3-\delta}$ membranes, *J. Membrane Sci.* 2005,**262**, 20-26.

20. S. Lee, Y. Lima, E. A. Lee, $Ba_{0.5}Sr_{0.5}Co_{0.8}Fe_{0.2}O_{3-\delta}$(BSCF) and $La_{0.6}Ba_{0.4}Co_{0.2}Fe_{0.8}O_{3-\delta}$(LBCF) cathodes prepared by combined citrate-EDTA method for IT-SOFCs, *J. Power Sources* 2006,**157**, 848-854.

21. W. Zhou, Z. Shao, R. Ran, Z. Chen, High performance electrode for electrochemical oxygen generator cell based on solid electrolyte ion transport membrane, *Electrochim. Acta.* 2007, **52**, 6297-6303.

22. M.A.Pena, J.L. Fierro, Chemical structures and performance of perovskite oxides. *Chem. Rev.* 2001, **101**, 1981-2017.

Figure Captions：

Figure 1. Scheme for O_2/CO_2 production integrated oxy-fuel combustion process.

Figure 2. Schematic diagram of fixed-bed reaction system. (1) Gas cylinder; (2) valve; (3) flow controller; (4) thermocouple; (5) temperature controller; (6) quartz reactor; (7) horizontal tube furnace; (8) gas analyzer; (9) data acquisition system.

Figure 3. Oxygen adsorption curves for A (A=Sr, Ba, Mg, Ca) $Co_{0.8}Fe_{0.2}O_{3-\delta}$

Figure 4. Oxygen desorption curves for A (A=Sr, Ba, Mg, Ca) $Co_{0.8}Fe_{0.2}O_{3-\delta}$

Figure 5. Oxygen desorption curves of $BaCo_{0.8}Fe_{0.2}O_{3-\delta}$ at different desorption temperatures

Figure 6. Oxygen desorption curves of $BaCo_{0.8}Fe_{0.2}O_{3-\delta}$ at different CO_2 partial pressure at 850 ℃

Figure 7. Comparison of oxygen adsorption capacity for $SrCo_{0.8}B$ (B=Fe, Ni, Cu, Zn, Cr, Zr) $_{0.2}O_{3-\delta}$

Figure 8. Comparison of Oxygen desorption amount for $SrCo_{0.8}B$ (B=Fe, Ni, Cu, Zn, Cr, Zr $)_{0.2}O_{3-\delta}$ with the number of cycles.

366 **Figure 1.**

367

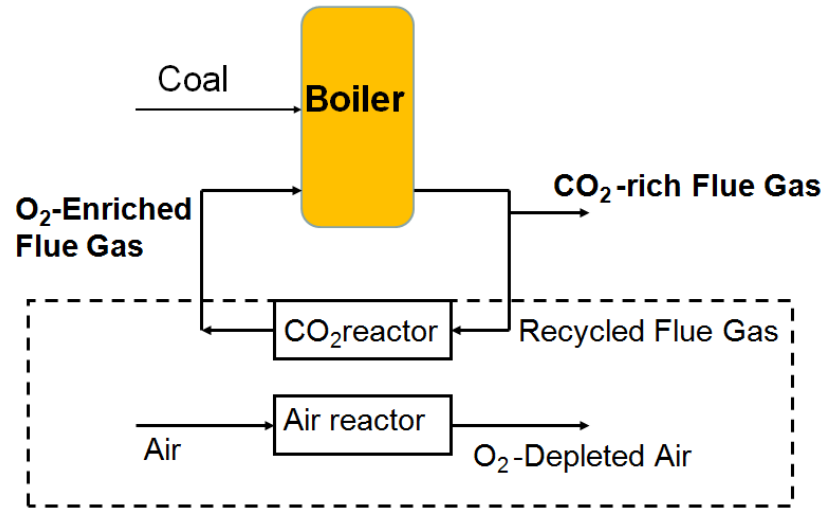

368

369

370

371

372

373

374 **Figure 2.**

375

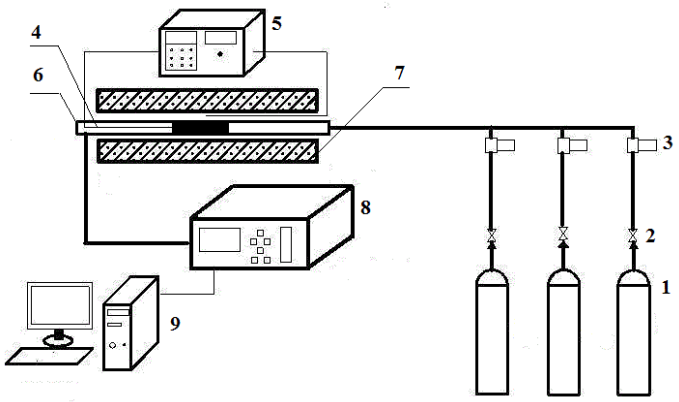

376

377

Figure 3.

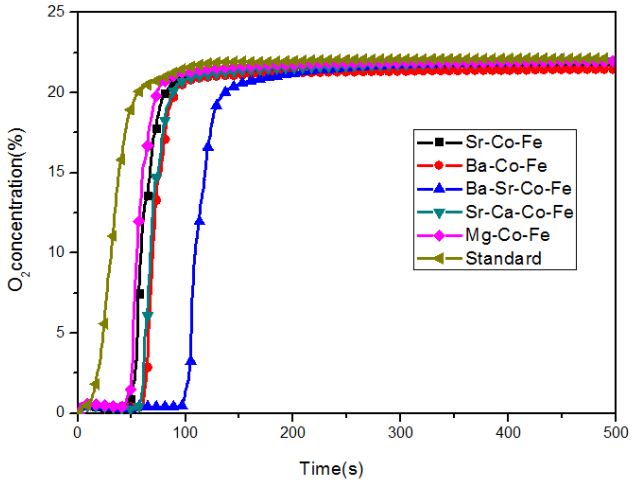

Figure 4.

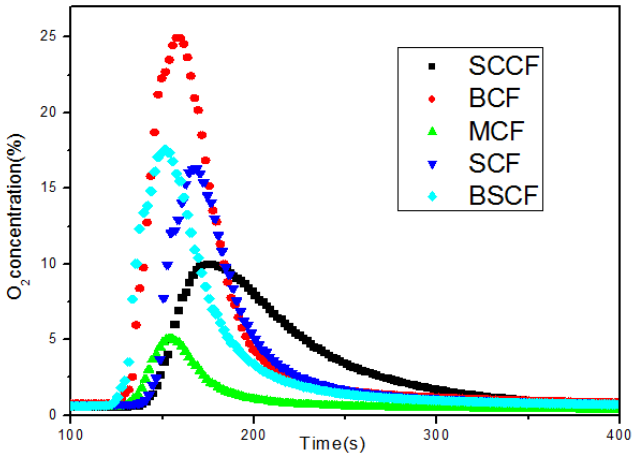

389 **Figure 5.**

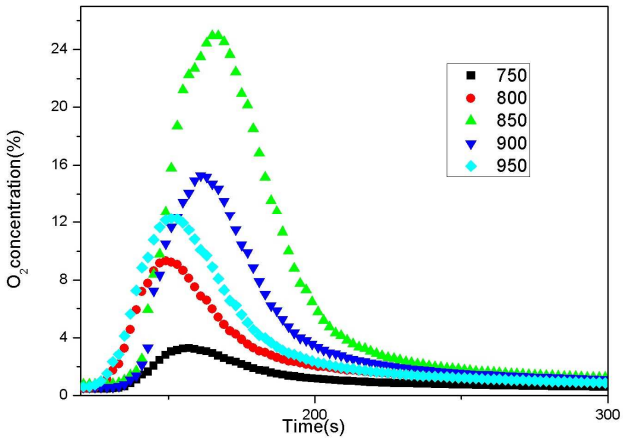

390

391

392 **Figure 6.**

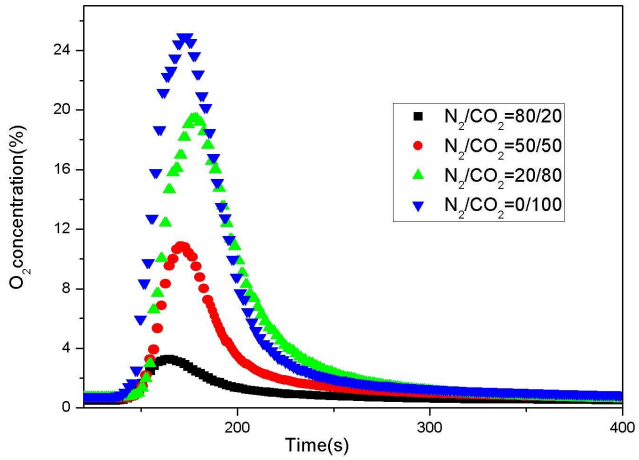

393

394

395

396

397

398 **Figure 7.**

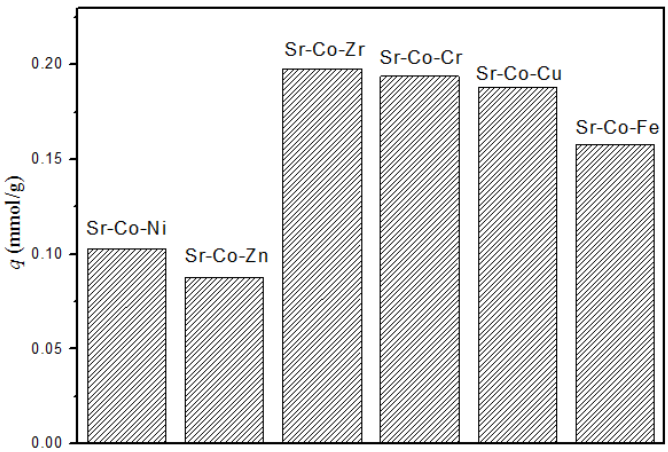

399

400

401 **Figure 8.**

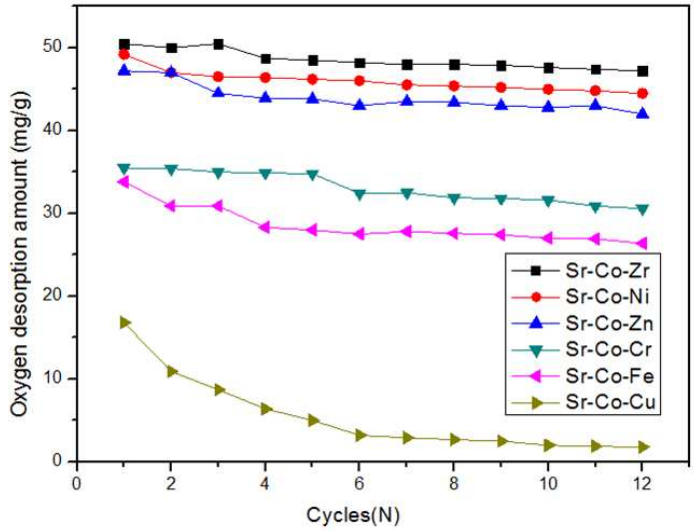

402